



American Society of
Mechanical Engineers

ASME Accepted Manuscript Repository

Institutional Repository Cover Sheet

Cranfield Collection of E-Research - CERES

First

Last

ASME Paper Title: Forcing boundary-layer transition on a single-element wing in ground effect

Authors: Luke S. Roberts, Mark V. Finnis and Kevin Knowles

ASME Journal Title: Journal of Fluids Engineering

Volume/Issue Vol. 139, Iss. 10 Date of Publication (VOR* Online) 21.7.2017

ASME Digital Collection URL: <http://fluidsengineering.asmedigitalcollection.asme.org/article.aspx?articleid=2633198>

DOI: 10.1115/1.4037036

*VOR (version of record)

Forcing boundary-layer transition on a single-element wing in ground effect

Luke S Roberts¹

Email: l.roberts@cranfield.ac.uk
Cranfield University

Mark V Finnis¹

Email: m.v.finnis@cranfield.ac.uk
Cranfield University

Kevin Knowles¹

Email: k.knowles@cranfield.ac.uk
Cranfield University

ABSTRACT

The transition from a laminar to turbulent boundary layer on a wing operating at low Reynolds numbers can have a large effect on its aerodynamic performance. For a wing operating in ground effect, where very low pressures and large pressure gradients are common, the effect is even greater. A study was conducted into the effect of forcing boundary-layer transition on the suction surface of an inverted GA(W)-1 section single-element wing in ground effect, which is representative of a racing-car front wing. Transition to a turbulent boundary layer was forced at varying chordwise locations and compared to the free-transition case using experimental and computational methods. Forcing transition caused the laminar separation bubble, which was the unforced transition mechanism, to be eliminated in all cases and trailing-edge separation to occur instead. The aerodynamic forces produced by the wing with trailing-edge separation were shown to be dependent on trip location. As the trip was moved upstream the separation point also moved upstream, this led to an increase in drag and reduction in downforce. In addition to significant changes to the pressure field around the wing, turbulent energy in the wake was considerably reduced by forcing transition. The differences between free- and forced-transition wings were shown to be significant, highlighting the importance of modelling transition for ground-effect wings. Additionally, it has been shown that whilst it is possible to reproduce the force coefficient of a higher Reynolds number case by forcing the boundary layer to a turbulent state, the flow features, both on-surface and off-surface, are not recreated.

¹ Aeromechanical Systems Group,
Centre for Defence Engineering
Cranfield University
Defence Academy of the United Kingdom
Shrivenham, SN6 8LA, UK

1. INTRODUCTION

The action of forcing transition from a laminar to a turbulent boundary layer is common during wind tunnel testing to eliminate the later transition caused by testing at reduced Reynolds numbers [1]. Above a critical Reynolds number, premature transition can be promoted through mechanisms that artificially introduce perturbations into the flow with a view to increasing momentum thickness at that point and generating turbulence. In the present work, perturbations are created through disturbances from a roughness-type strip.

Monoposto racing cars generate downforce through the use of inverted wings. It has been comprehensively shown that as the distance between a wing and the ground decreases the wing will generate more downforce as flow is constrained between it and the ground, hence increasing suction levels [2-8]. This phenomenon is true down to a critical ground clearance, below which the flow can no longer overcome the large adverse pressure gradient associated with the increased suction level and separates. This gives what is known as the force-reduction region. Correia et al. [8], however, showed, with the same wing as used in the present study, that the force-reduction mechanism is not only caused by the stalling of the wing but also is due to a de-cambering of the wing's effective shape. This de-cambering effect is due to the separation bubble, which displaces the streamlines from the surface to alter the wing's effective shape, becoming smaller and thinner and thus reducing its influence on the wing.

The front wing of a racing car is the first component to interact with the oncoming air. Therefore, in addition to generating aerodynamic downforce its primary functions are to provide high-energy flow to downstream features, maximise mass flow into the underbody and control the front tyre wakes. These functions are wake-structure based, and therefore the development of an aerodynamic design for a racing car is reliant on accurate representation of the front wing flow structures during wind tunnel testing.

The use of boundary-layer trips in order to force the transition from a laminar to a turbulent boundary layer has been widely reported in the aeronautical sector [9-12]. However, the use of trips has been reported only for single locations in ground-effect cases [7, 8]. In both these latter studies, forced transition caused a reduction in downforce. A reduction in the downforce produced by the wing would also imply a reduction in upwash, hence changing the wake structure behind the wing.

Transition on an inverted wing in ground effect has been shown to occur through a laminar separation bubble [7, 8]. A separation bubble, a schematic of which is given in Figure 1, forms on a wing when the laminar boundary layer separates due to the adverse pressure gradient. Kelvin-Helmholtz type instabilities then grow in the separated shear layer causing turbulence production. Increased mixing and entrainment of higher velocity flow causes reattachment to the wall and subsequent development of a turbulent boundary layer. The act of tripping the boundary layer prior to the pressure recovery bypasses the formation of this bubble.

Correia et al. [8] showed that the presence of a separation bubble altered the effective shape of the wing to aid in downforce production. It was found that the bubble re-energised the boundary layer on reattachment to help it overcome the adverse pressure gradient. The elimination of this bubble through the use of a roughness-type trip located $0.25c$ from the leading edge caused a reduction in downforce.

Zerihan & Zhang [7] observed a loss of downforce coefficient from $C_L = 1.72$ to $C_L = 1.15$ when a roughness-type trip was placed $0.1c$ from the leading edge of a Tyrrell-026-section wing due to the reduction in both pressure and suction on their respective surfaces. Trailing-edge separation was shown to increase for forced-transition tests, which the authors stated as being due to a thicker boundary layer being present in the adverse pressure gradient region. A laminar separation bubble was declared as the transition mechanism for this wing, however, no further investigation regarding its occurrence was reported.

The present work investigates the effect of forcing transition at varying chordwise locations on the suction surface of a single-element inverted wing in ground effect, using a range of computational and experimental methods. The overall aim of the work is to provide further insight into the practise of forcing transition for wing-in-ground-effect cases and establish the importance of understanding and modelling transition mechanisms in further studies.

2. DESCRIPTION OF STUDY

2.1 Test facility

Experiments were conducted in Cranfield University's DS Houghton wind tunnel at the Defence Academy of the United Kingdom, Shrivenham. This is a 2.7m x 1.7m closed-return, three-quarter-open test section wind tunnel with freestream turbulence of 0.3%. A continuous-belt rolling road synchronized with the freestream velocity allows correct representation of the wing moving over a stationary road. Boundary-layer suction is applied through perforated plates ahead of the rolling road to remove the test-section boundary layer. The optimisation and distribution of this suction coupled with a knife-edge transition to the road's belt gives a residual boundary-layer thickness of only 1.58mm at the leading edge of the model. The model is supported by an overhead sting that incorporates an automated motion control system to adjust accurately the model's ground clearance to the rolling road throughout the experiment. Further information on this tunnel is given by Knowles & Finnis [14].

2. Test Model

Tests were conducted on an untapered, untwisted, rectangular-planform, GA(W)-1 section single-element wing of span 750 mm and chord 119.7 mm, set at -0.5° incidence, with endplates from a double-element wing configuration fitted parallel to the road (Figure 2a). These dimensions mean that the model is approximately a 50% scale representation of a post-

2009 Formula-One front wing main plane. It is, however, also representative of junior-series racing cars such a Formula 4, in which single-element wings are used. The wing was suspended by two fixed vertical pylons from a six-component Aerotech force balance housed inside a non-metric streamlined body (Figure 2b). This streamlined body isolated the force balance from the airflow and simulated the nose cone of a Formula-type racing car.

2.3 Experimental Method and Uncertainties

Force measurements were taken at a range of ground clearances, defined as the distance from the lowest point of the wing's suction surface to the road. The model was positioned to an accuracy of $\pm 0.0037^\circ$ in roll, $\pm 0.0015^\circ$ in incidence, and $\pm 0.0019^\circ$ in yaw. The wind tunnel was run at a constant chord-based Reynolds number, with an uncertainty of ± 470 ; in this mode the control system adjusts the velocity such that the Reynolds number remains constant even if the ambient temperature and pressure change. The tested Reynolds number range was $Re = 1.63 \times 10^5$ to $Re = 2.44 \times 10^5$; these Reynolds numbers are low compared to that which would be attained on track due to the model scale and tunnel speed. This has implications for the boundary-layer thickness, transition and separation characteristics, and force coefficients. An investigation into Reynolds-number scaling effects and initial use of boundary-layer trips on the same geometry used in this study was previously completed by Correia et al. [8]. Given that Correia et al. primarily focussed on $Re = 2.03 \times 10^5$, the Reynolds number range was extended for the present study.

Force data were acquired at a frequency of 10 Hz for 20 seconds at each ground clearance. Nil-force (wind-off) data were acquired before and after each experiment to account for any offsets in the measurements during the experiment. This was done to ensure any change in ambient conditions, such as temperature, during the run had not significantly altered the force-balance reading. Although the difference between the nil-force readings was always less than

1%, the difference was accounted for when subtracting the nil-force (wind-off) measurement from the wind-on measurement.

The uncertainties in drag and lift coefficient measurements were calculated at a 95% confidence level to be 0.002 and 0.014 respectively. This calculation accounted for all variables affecting the experiment such as pitch, roll, yaw, dynamic pressure, ground clearance, and force balance error. The uncertainty associated with each variable was calculated by doing a parametric study where each variable was changed individually and tested at two different settings. It was then assumed that the resultant variation caused by each variable was linear between the two tested settings. The total uncertainty values (stated above) were then calculated by combining the uncertainties for each variable with the force-balance uncertainty using the root-mean-square method, as described by Moffat [15].

Forced-transition tests were conducted using roughness-type strips of streamwise length 0.1c placed at varying distances from the leading edge with an accuracy of $\pm 0.0042c$. These trips were chosen as they had been utilised in a previous study of this test model by Correia, et al. [8]. The leading edge of the trip is considered to be the datum line. Using the procedure proposed by Braslow and Knox [16] a grit size of 265 μm (grit 60) was calculated as the requirement to cause transition. Additionally, the grit size satisfied the roughness-based Reynolds number criterion required for transition [17]. Further detail on the mechanism by which roughness-type strips induce transition can be found in Klebanoff & Tidstrom [18].

Surface flow visualisation tests were conducted using a paint consisting of fluorescent pigment, oleic acid and paraffin applied to the suction surface of the wing. The paint was sprayed onto the wing and then the flow pattern allowed to dry for 45 minutes while the wind tunnel was run at constant Reynolds number. Once the flow pattern was dry the wing was removed to a dark-room and photographs taken under ultra-violet light.

2.4 Two-dimensional coupled viscous-inviscid simulations

In order to observe the effect of forced transition without three-dimensional effects, and gain further insight into the boundary-layer characteristics, 2D computations in MSES was undertaken. MSES (Multi-element Streamline Euler Solver) is a two-dimensional flow solver developed to allow for the design and analysis of multi-element airfoils [18, 19]. The solution is based on the inviscid Euler equations coupled, through displacement thickness, with a two-equation boundary-layer formulation and solved simultaneously using the Newton method.

Laminar-to-turbulent transition is predicted by a simplified variant of the e^N method [21], known as the envelope method, which determines the amplitude of the most amplified Tollmien-Schlichting wave frequency at each point. The premise is that when the spatial amplification of disturbances reaches a critical point transition will occur. Smith & Gamberoni [22] correlated the transition point found in experiments with the real part of the Orr-Sommerfeld eigenvalue and determined that when disturbances had grown approximately 8000 times (e^9) transition would occur. Van Ingen [21] suggested that lower values of e^7 or e^8 should be used. Mack [23] suggested that the critical amplification factor (N) could be calculated from the wind tunnel freestream turbulence intensity through Eqn. 1. Using the DS Houghton's freestream turbulence intensity of $Tu = 0.3\%$, a critical amplification factor of $N = 5.51$ was calculated.

$$N = -8.43 - 2.4 \ln \left(\frac{Tu}{100} \right) \quad (1)$$

MSES allows the transition point to be specified, thus simulating boundary-layer trips. This enforces a turbulent boundary layer from this point unless the $e^{5.51}$ criterion has already been fulfilled upstream and natural transition has occurred. The ground plane was computed through use of the mirror-image technique. This technique is an established concept for simulating the presence of a moving ground in wind tunnels. The method involves two identical geometries positioned such that they are mirror images of each other, with the ground then being

represented by the horizontal plane of symmetry. As such it does not account for the residual boundary layer which forms due to the velocity gradient normal to the floor.

2.5 Three-dimensional RANS simulations

Due to the lack of off-surface measurements in both MSES and experimental tests, and the lack of pressure measurements on the wind tunnel model, RANS computational analysis of the free-transition and forced-transition at $x/c = 0.1$ was undertaken to fill these gaps. Validation was conducted by comparing the prediction of sectional forces and surface streamlines to the experimental results. Additionally, Correia et al [24] used the same turbulence model and a similar RANS method to that of the present study and showed good agreement with flow-field LDA measurements from the DS Houghton wind tunnel.

Simulations were conducted using the commercial software ANSYS Fluent 15.0.7 [25] on Cranfield University's high-performance computing network, Astral. This is a dedicated cluster of nodes with a total of 1280 cores available and a peak measured performance of 18.8 TFlops. In the present study, 64 CPU cores and 256 GB of shared memory were used. The geometry was discretised into 3.2×10^7 unstructured surface and volume elements in a domain spanning 3X upstream and 7X downstream from the model (whose length is X), a total width of 6X, and height of 3X – giving a blockage of 3.7%. The domain was large enough that constant pressure was maintained on all boundaries, hence showing that the model was not interacting with them. Of the total elements approximately 1.2×10^6 were triangular surface elements, 1.8×10^7 prism boundary-layer elements and 1.3×10^7 tetrahedral volume elements. In order to allow simulation of both free and forced transition the domain was split into two cell zones, as shown in Figure 3, the laminar zone and turbulent zone, with an interior wall positioned $0.1c$ downstream of the leading edge separating them. The same grid generation parameter were used for both zones.

To keep $Y^+ < 1$ across the wing a target Y^+ of 0.8 based on main-plane chord length and freestream values was imposed during meshing. A total of 21 prism layers, with a 1.2 growth rate, were used to ensure the full boundary layer was contained in the prism elements and to limit the difference in cell volume at the interface between prism and volume elements. Volume elements around the wing were refined to ensure accurate prediction of the off-surface flow structures and minimise the truncation error of the discretisation causing artificial dissipation of the vortices. The mesh, which can be seen in Figure 3, is fine enough to eliminate grid dependency, as was concluded through a mesh-dependence study. This study showed that simply refining to the viscous sublayer $1 < Y^+ < 5$ was not adequate, and instead required $Y^+ < 1$. The number of prism layers was set so that the boundary layer was fully encompassed inside the prism elements. This defined the large number of surface and prism layer elements required. Whilst smaller meshes, with the same surface and prism element method, were found to give the same forces and surface streamlines it was decided that the mesh with more volume refinement should be used due to the lack of suitable off-surface validation. Additionally, the finest tested mesh was deemed acceptable due to the lack of computer time constraints for this work.

Additional prism layers were placed on the ground below the wing in order to capture the boundary layer which forms there. This is required because a velocity gradient is created between the ground, which moves at the same velocity as the freestream air, and the accelerated flow that is constrained between the wing and the ground. A total of 10 prism layers, with a 1.2 growth rate, with a $Y^+ < 1$ were placed on the ground as shown in Figure 3b. Simulations were conducted with and without the prism layers on the ground to understand their influence on the final solution.

A steady-state, incompressible, segregated solver was used. The same mesh (Figure 3) was used for both free- and forced-transition simulations. For free-transition simulations the

k - k_L - ω turbulence model was imposed in both cell zones. This model is based on k - ω but includes an additional transport equation. It was used as it is capable of predicting laminar-turbulent transition through the inclusion of a laminar kinetic energy term. For the forced-transition case the upstream cell zone was set as laminar, and the downstream cell zone imposed with the fully-turbulent k - ω SST model. The laminar zone disables turbulent production, but still transports the turbulence quantities that were defined at the inlet, thus allowing turbulent viscosity to be calculated in the laminar zone. The k - ω SST model, as it is the fully-turbulent model which most closely resembles the k - k_L - ω model (the addition of a third transport equation being the primary difference), was thus deemed the most applicable. To limit the effect of numerical diffusion on the accuracy of the results 2nd-order upwind numerical schemes were used for the discretisation of momentum, k , k_L , and ω . Pressure and velocity fields were coupled using the SIMPLE scheme and computation of cell gradients completed with a Green-Gauss node-based scheme.

The boundary conditions used in the simulation are indicated in Figure 3a. Flow entered the computational domain through a velocity inlet. Turbulence was specified by turbulent intensity and turbulent length scale at the inlet for both free- and forced-transition cases, values of $k = 1.215 \text{ m}^2\text{s}^{-2}$, $k_L = 10^{-6} \text{ m}^2\text{s}^{-2}$ (where applicable), and $\omega = 2.012 \text{ s}^{-1}$ were defined. Symmetry conditions were applied to the upper and side boundaries, and a moving wall, with the same magnitude as the freestream wind velocity, to recreate the rolling road. Flow then left through a pressure outlet. Simulations were initialised with a zero-velocity flow-field and run for 12,000 iterations. A high number of iterations was used because under-relaxation factors were kept low to promote numerical stability whilst ensuring that lift and drag coefficients had become steady-state ($\pm 10^{-4}$), and residuals were below 10^{-5} .

3. EXPERIMENTAL RESULTS

Observations of the effect of forced transition on a three-dimensional wing in ground effect were conducted through experimental testing. The trip location was varied between $0.1c$ and $0.5c$ at $0.1c$ intervals for force measurements, and at $0.1c$, $0.3c$, and $0.5c$ for flow visualisation tests. The experiment was divided into two sections: firstly, the measurement of aerodynamic forces; and secondly, the observation of surface flow mechanisms through surface oil flow visualisation.

3.1 Force measurements

Figure 4 contains the force curves for the wing in both free- and forced-transition at various Reynolds number. The free-transition wing at $Re = 2.03 \times 10^5$ shows the classic wing-in-ground-effect behavior: downforce increases with reducing ground clearance, until a maximum downforce is reached and the force-reduction region is entered at low ground clearances. At $Re = 1.63 \times 10^5$ the force-reduction region occurs at a higher ground clearance with negligible prior force enhancement, whilst the $Re = 2.44 \times 10^5$ case shows no force-reduction region. Both are a consequence of the change in kinetic energy allowing the boundary layer to overcome (or not overcome) the adverse pressure gradient. The effect of trip location provides a fairly consistent trend across all ground clearances and Reynolds numbers, whereby the curve shape appears the same, but the magnitude of downforce is increased as the trip is moved downstream. The key difference is that at $Re = 1.63 \times 10^5$ the forced-transition cases produce significantly more downforce than the free-transition wing, because there is no force-reduction phenomenon in the tested ground clearance range for forced-transition cases. At $Re = 2.44 \times 10^5$, where force reduction does not occur for the free-transition wing, the tripped cases give less downforce. The $Re = 2.03 \times 10^5$ case represents a median because force-reduction occurs, but at a much lower ground clearance than for $Re = 1.63 \times 10^5$; at the lowest

tested ground clearance, however, all forced-transition cases produce more downforce. Comparison of the behavior of the $0.5c$ trip at $Re = 1.63 \times 10^5$ to the free-transition wing at $Re = 2.44 \times 10^5$ shows them to be similar in terms of both trend and magnitude, thus showing it is possible to make a lower Reynolds number case act like a higher Reynolds number case, at least in terms of aerodynamic force. Whilst the free-transition case shows substantial Reynolds number dependency, comparison of each trip location at the various Reynolds numbers shows that the forced-transition wings are very much insensitive to Reynolds number. This shows why at lower Reynolds numbers the forced-transition cases produce more downforce than the free-transition case, and less at higher Reynolds numbers.

The drag coefficient, similar to downforce for the forced-transition cases, is observed to show an insensitivity to Reynolds number. The drag curves show an opposing trend to downforce in that the forced-transition cases produce less drag, at all ground clearances, at lower Reynolds numbers, but at the higher Reynolds numbers more drag is produced. The overlying trend, however, is that the more upstream position the boundary-layer trip is placed, the higher the drag at any given ground clearance. Additionally, as the ground clearance reduces the drag curves for all trip locations converge.

The effect of trips seems to be amplified by the ground clearance, as Zerihaan & Zhang [7] also reported, most likely due to the way the turbulent boundary layer interacts with the larger adverse pressure gradient produced close to the ground, hence dramatically changing the force-reduction region. In the range $0.5 < h/c < 2$ the change in drag force is fairly linear; however, below $h/c = 0.5$ there is a dramatic reduction in drag. Given that the force-reduction region of the free-transition wing does not occur until $h/c = 0.209$ it shows ground effect altering some characteristics non-linearly.

3.2 Flow Visualisation

Suction-surface flow visualisation results at $Re = 1.63 \times 10^5$ and $Re = 2.44 \times 10^5$ at $h/c = 0.3125$ for the free-transition and forced-transition cases are given in Figure 5. The two free-transition cases are defined by the existence of a laminar separation bubble; this is seen as the area where the paint has not been moved, as there is no x-component of shear stress inside the bubble. At this ground clearance the $Re = 1.63 \times 10^5$ case is in the force-reduction region. The flow visualisation shows that this occurs because the boundary layer does not fully reattach, hence circulation is reduced and as a result downforce is lost. Full reattachment of the turbulent boundary layer occurs for $Re = 2.44 \times 10^5$, hence why it remains in the force-enhancement region at this ground clearance.

At both tested Reynolds numbers the forced-transition cases display close similarity, thus showing why little Reynolds-number sensitivity was displayed for such cases. The act of forcing transition to a turbulent boundary layer eliminates the formation of the laminar separation bubble, as no laminar boundary layer encounters the adverse pressure gradient. The turbulent boundary layer is more capable of overcoming the adverse pressure gradient, since the fluctuating velocity components provide momentum transfer normal to the wall, and it remains attached longer. For the $x/c = 0.1$ and $x/c = 0.3$ trip locations the adverse pressure gradient cannot be overcome over the full chord and turbulent trailing-edge separation occurs. The $x/c = 0.1$ case displays the most separated flow; as the trip is then moved downstream the separation point also moves downstream. Correia et al. [8] pointed out that the separation bubble effectively resets the boundary layer, thus allowing it to overcome the adverse pressure gradient without separating. Therefore, by forcing the boundary layer to become turbulent prematurely this cannot occur. The turbulent boundary layer for the free-transition case begins upon reattachment of the separated shear layer, whilst for the forced-transition cases the turbulent boundary layer must cover up to $0.9c$ of the surface; this means that it loses more

energy and makes separation more likely. For the $x/c = 0.5$ trip location no trailing-edge separation occurs, thus demonstrating why no force-reduction region was observed. In fact, it appears that a separation bubble is still being produced: shown by the build-up of paint behind the trip for $Re = 1.63 \times 10^5$ and the dark shade behind both. Given that the apex for the GA(W)-1 profile is at $x/c = 0.42$, the $x/c = 0.5$ trip is in the adverse pressure gradient. It can be postulated, therefore, that the trip is causing the laminar boundary layer to separate; the separated shear layer then quickly transitions and reattaches. Transition occurs quickly as the bubble is located at a point further upstream than the free-transition case, where flow velocities are higher. This means that the Kelvin-Helmholtz instabilities, which cause transition, are greater and thus the bubble is smaller. Correia et al. [8] showed that the bubble increases downforce as it allows higher suction levels to be maintained across the wing's surface; therefore, by occurring sooner a greater suction value is maintained and downforce increased.

The reason for the lack of Reynolds-number sensitivity for the forced-transition wing has already been touched upon. This, however, also explains why the trips allow the wing to produce more downforce than the free-transition case at the lower Reynolds numbers, but less at the higher Reynolds number. For free transition at $Re = 1.63 \times 10^5$ the separation occurs much further upstream, as it is the laminar separation point, and the turbulent nature of the boundary layer has allowed it to remain attached, thus increasing downforce. In contrast, however, for $Re = 2.44 \times 10^5$, where the boundary layer for the free-transition wing remains fully attached, the occurrence of trailing-edge separation only acts to reduce circulation and consequently reduce downforce. For the trip at $x/c = 0.5$, however, there is no turbulent trailing-edge separation, and thus this case produces a similar downforce curve to the free-transition wing. It is only the force-enhancement due to the bubble altering the effective camber of the wing that results in it producing slightly less downforce.

The force results for the minimum tested ground clearance ($h/c = 0.15$) and minimum tested Reynolds number ($Re = 1.63 \times 10^5$) showed the largest difference between free- and forced-transition of all test cases. Flow visualisation of this case is shown in Figure 6. In free transition (Figure 6a) there is a large area of recirculation near to the trailing edge. Based on the very low downforce this case produces, it appears that a fully-laminar separation occurs. The reverse vortex that occurs downstream of the laminar separation point still exists, hence the build-up of paint that resembles a bubble. After the reverse vortex, however, there is no attached flow and thus the paint has run due to gravity. The fully-laminar separation causes a significant loss of circulation and subsequent reduction in downforce. For forced transition at $x/c = 0.1$ and $x/c = 0.3$ there is still a small trailing-edge separation, however, it is significantly smaller than that of the free-transition case. Hence the incremental increase in downforce as the trip is moved downstream in Figure 4a. The $x/c = 0.5$ trip produced the most downforce of all cases. It can be seen from Figure 6d that this is because no trailing-edge separation occurs. The trip causes laminar separation, but aids in turbulence production such that turbulent reattachment occurs, and a large separation bubble being produced.

At low Reynolds numbers and low ground clearances the trips have much more influence as they prevent force-reduction phenomena by keeping the boundary layer attached longer. This allows a force similar to a higher Reynolds number, where force reduction does not occur, to be produced. The surface-flow structures are, however, notably different due to the lack of a separation bubble in the forced-transition case.

Although reducing ground clearance appears to amplify the effect of the trips, even at the highest test ground clearance the trips had a notable effect on the force coefficients. It is the chordwise size of the laminar boundary rather than the presence of the separation bubble that is the most influential. This is demonstrated by the notable differences between the forced-transition cases at $0.1 \leq x/c \leq 0.4$, as no separation bubble occurs in these instances.

3.3 MESES (2D) Computational Results

The change in sectional forces for the GA(W)-1 airfoil section at varying trip locations in comparison to the free-transition wing is given in Figure 7. This shows a similar trend to the experimental force results in that, for this ground clearance ($h/c = 0.3125$), downforce has been reduced overall by forcing transition, and as the trip location is moved upstream the downforce is lower. Drag has a more complicated trend whereby more drag than the free-transition wing is produced by the upstream trips, and less by the downstream trips. Although this is not the same as that observed in the experiments, it could stem from the difference between a two-dimensional airfoil geometry and a three-dimensional wing geometry. The two-dimensional simulation relies solely on pressure drag and skin friction drag, whilst the wing used in the experiments is also subject to vortex-induced drag from the wing tips. Such vortices also contribute to downforce as they induce a suction on the lower surface of the wing [24]. Zhang, et al.[24] also showed that at higher ground clearances a concentrated vortex core occurs, but at a lower ground clearance it bursts, though the wing does not necessarily enter the force-reduction region, and its contribution to downforce reduces and contribution to drag increases.

Correia et al. [8] cited the reduction in downforce for forced-transition cases as being due to an effective de-cambering of the airfoil shape as a result of the elimination of the laminar separation bubble. Based on this, it is postulated that the thicker boundary layer resulting from an earlier trip location is having a similar de-cambering effect. The trailing-edge separation causes a reduction in curvature, as shown visually in Figure 8 and confirmed by the increase in displacement thickness at the trailing edge in Figure 9c. By reducing this curvature the diffuser effect is also decreased and as a result mass flow, and subsequently flow velocity, underneath the wing reduces causing a loss of downforce. The loss of circulation changes the upwash component and thus alters the wake structure. The influence of the separation bubble on the airfoil's pressure distribution can be seen in Figure 9a as the region of constant pressure. This

shows why the bubble is a force-enhancement mechanism, as the area under the curve is now greater, and thus the downforce must be greater. This constant pressure is due to local flow separation associated with the separation bubble. As the boundary layer reattaches to the surface the strong local flow curvature causes the pressure to recover quickly towards the inviscid pressure distribution. The alteration to the local flow curvature, which is a result of the separation bubble, is shown in Figure 8. The reduction in downforce with more upstream trip locations can be seen by the lower suction values attained in those cases. It is the elimination of the bubble which causes all forced-transition cases to have lower downforce than the free-transition wing, as can be seen in the pressure distributions.

The streamlines in Figure 8 show that a thicker wake is produced when the boundary layer is tripped at a more upstream location. This is confirmed by observation of the displacement thickness in Figure 9c. The boundary layer displacement thickness shows that the more upstream trips lead to a thicker turbulent boundary layer, however this is only observed under the adverse pressure gradient i.e. the aft section of the wing. The free-transition wing gives the thinnest boundary layer at the trailing edge. The skin friction coefficient, which is plotted in Figure 9b, shows where the turbulent boundary layer begins. In free transition, the laminar boundary layer exists until it separates at $x/c = 0.614$, the extent of the separation bubble then is shown by the area of zero skin friction²; a result of the boundary layer having separated from the surface. The turbulent boundary layer then begins upon reattachment at $x/c = 0.784$ where the skin friction coefficient begins to grow once again. For the forced-transition cases, the rise in skin friction coefficient above that of the laminar boundary layer (free-transition cases) indicates the point at which the boundary layer has become turbulent. Given that the area underneath the skin friction curve is equivalent to the friction drag of the wing, it can be seen

² Figure 8b has been cropped to $C_F = 0$, the bubble contains reverse flow (as shown in Figure 1) and thus exhibits small negative values of C_F if left uncropped.

why the more upstream trip locations produce higher drag forces. The higher skin-friction values at the trailing edge for the more downstream trip locations, and for the free-transition case, show that the boundary layer is further from separation. This is in line with that seen in the previous section, where tripping the boundary layer prematurely makes separation more likely. The earlier trip locations increase separation likelihood as the rate of momentum diffusion is greater in a turbulent boundary layer. This momentum loss is an energy removal, meaning that the flow cannot overcome the adverse pressure gradient as easily and causes it to separate.

The momentum thickness, which is shown (in the form of Re_θ) in Figure 9d, is the distance the boundary layer must be displaced to compensate for the reduction in momentum of flowing fluid on account of the boundary layer formation. Essentially it shows us the momentum deficit across the boundary layer. Tripping the boundary layer causes an increase in momentum thickness from that point, which is understandable given the turbulent boundary layer that is created. Thus, the higher Re_θ values of the upstream trip locations show the momentum loss alluded to. Moreover, as Re_θ is a measure of total drag, if the area under the Re_θ curves is observed it can be seen that the more upstream trip locations produce the highest drag, but additionally, the more downstream trip locations produce less drag than the free-transition case; as was seen in Figure 7. Based on the Re_θ curves it can be inferred that, by the boundary layer becoming turbulent in the favourable pressure gradient turbulence production is suppressed, thus when the turbulent boundary layer of the free-transition case reattaches a much sharper rise in Re_θ is seen.

3.4 RANS (3D) Computational Results

The previous sections have shown that forcing boundary-layer transition has a considerable effect on the sectional forces and surface-flow characteristics of the wing. Due to the lack of

off-surface flow measurements available for the present wind tunnel test configuration a computational investigation was also conducted. Validation of the computational approach in terms of aerodynamic forces and surface flow structures are given in Table 1 and Figure 10. In both cases drag is under-predicted and downforce over-predicted by the CFD. For the free-transition case the $k-k_L-\omega$ model is capable of predicting the occurrence of a laminar separation bubble. The bubble occurs more downstream in the simulation than in the wind tunnel tests; the length of the bubble, however, was predicted accurately. For the forced-transition case trailing-edge separation occurs, and the point of separation is closely predicted.

Observation of the pressure distribution for the free- and forced-transition cases, in Figure 11, shows that the forced-transition case produces less downforce due to a reduction in surface pressure on the upper surface, and a reduction in suction on the lower surface. The magnitude of the suction in comparison to that of pressures means that the reduction in suction has a more significant effect on the total downforce level. As discussed previously, the bubble alters the effective shape of the wing akin to an increase in camber, thus increasing circulation. This leads to the suction levels across the entire suction surface being increased. The x-component of shear stress shows similar trends to those found in the previous section using MSES. In free transition the shear stress reduces along the wing, becoming zero where the laminar boundary layer separates and then increasing again once the turbulent boundary layer reattaches. In the forced-transition case, the shear stress deviates from that of the laminar boundary layer shortly after being tripped to a turbulent state at $x/c = 0.1$. After this initial rise of shear stress, it then decreases until the boundary layer separates at $x/c \approx 0.9$, as shown by the zero shear stress values.

Table 1 - Downforce and drag coefficients, and boundary-layer separation and reattachment locations for free- and forced-transition wing from experiments and CFD.

	Method	C_D	$-C_L$	Separation (x/c)	Reattachment (x/c)
Free-transition	Experimental	0.0431	0.627	0.558	0.785
	RANS	0.0399	0.676	0.610	0.831
Forced-transition	Experimental	0.0469	0.476	0.934	-
	RANS	0.0432	0.553	0.926	-

The off-surface flow-field around the wing for the two cases is given in Figure 12; the left column shows the free-transition case, and the right column the difference between the two cases. Figure 12a and 12b show that the wing produces significant amounts of suction underneath it. The ΔC_P plot shows that the pressure field is significantly different for the two cases; showing that not only has the surface pressure altered, but the entire pressure field has been altered. Positive values of ΔC_P denote a higher pressure and negative values denote more suction, for the free-transition case. The main area of difference between the two occurs where the separation bubble appears at $x/c = 0.7$; this highlights the dramatic increase in local suction that the bubble causes.

The total pressure loss for the free-transition case, Figure 12c and 12d, allows the thickness of the separation to be viewed. As the boundary layer remains attached for the free-transition case the wake is not particularly large, at least in comparison to the forced-transition case. The trailing-edge separation of the forced-transition case leads to a much thicker wake, as shown by the positive values of ΔP_0 , which indicates greater total pressure loss. The inclusion of the laminar-separation bubble can be seen by the negative ΔP_0 values on the suction surface and the full extent of the change in effective shape due to the bubble can be seen. As the GA(W)-1 is an aft-loaded airfoil, forcing transition at $x/c = 0.1$ means that the turbulent boundary layer must travel through a large favourable pressure gradient. This acceleration of the flow

suppresses turbulence in the boundary layer, commonly termed relaminarisation. Although the boundary layer certainly does not become laminar again, this clearly has an influence on the turbulent kinetic energy. Hence, these results may have some airfoil geometry dependence, due to the favourable pressure gradient encompassing a larger portion of the GA(W)-1 than other airfoil shapes.

In the free-transition flow-field, turbulent kinetic energy (Figure 12e) is only produced downstream of $x/c = 0.7$, which is, as Figure 11 showed, approximately the center of the bubble. This is because upstream of this the turbulence model will have been using the laminar kinetic energy (k_L) term, then turbulent kinetic energy (k) is produced in the bubble due to instabilities growing the separated shear layer. In the forced-transition case turbulent kinetic energy is produced in the boundary layer from $x/c = 0.1$, which can be seen by the negative Δk values that occur prior to $x/c = 0.7$. The Δk contours, in Figure 12f, shows that significantly more turbulent kinetic energy is produced in the free-transition than in the forced case (Δk positive) downstream of $x/c = 0.7$. This is the result of turbulence being suppressed by the favourable pressure gradient in the forced-transition case, whilst in free transition all turbulence production occurs in the adverse pressure gradient. Comparing the values given in the free-transition case, it can be seen that almost twice as much turbulent kinetic energy is generated by the instabilities in the separation-induced transition event of the free-transition wing than the forced-transition event or trailing-edge separation of the forced-transition wing. It should be noted, however, that the inclusion of the significant surface roughness given by the trip used in the wind tunnel would have an effect on the level of turbulent kinetic energy; this is not captured in the RANS model.

4. CONCLUSIONS

The present work investigated how forcing the boundary layer to transition prematurely to a turbulent state on the suction surface of a single-element wing operating in ground effect affected the forces and surface flow structures. The forces produced and the trailing-edge separation position were shown to be dependent on the trip location. It was shown that this was due to trailing-edge separation reducing circulation by a degree dependent on the trip location, where separation occurred earlier for trips placed further upstream.

The study highlighted the importance of correct placement of boundary-layer trips, due to the large change in both force production and separation point with different trip locations, in order to achieve accurate representation in a wind tunnel of a full-scale wing. Despite roughness-type trips being capable of fixing transition to the earlier location which would occur at full-scale testing, the occurrence of trailing-edge separation and elimination of the separation bubble are not representative of that expected at full scale. In certain conditions the forces expected of a wing operating at a higher Reynolds number were observed, however it is not currently clear if this is achievable with different wing profiles as this requires further investigation.

Roughness-type trips simulated the occurrence of a bypass transition, which previous studies have shown occur on racing car wings operating in the turbulent wake of another car [24]. Such a situation has been simulated and observed in this study. There is still a question, however, as to whether the freestream turbulence level is high enough even at full-scale racing speeds (where Reynolds numbers are still relatively low) for bypass transition to precede separation-induced transition, other than in exceptional circumstance. The use of roughness-type trips here has shown bypass-style transition at varying locations along the wing, and thus gives an understanding of how the wing reacts to transition occurring at different locations due to different freestream turbulence magnitudes.

The significant differences in the pressure field and production of turbulent energy between the free- and forced-transition cases in addition to the surface-flow changes, due to the dramatic increase in suction levels from the separation bubble, highlighted the importance of modelling transition effects for wings operating in ground effect at low Reynolds numbers. The importance of ground effect in such a statement should not be overlooked as the large suction levels and strong pressure gradients that occur in ground effect make it markedly different from un-constrained aeronautical tests. Although forcing transition is usually conducted in order to give the earlier transition point of higher Reynolds number flows, the difficulty is that although the transition point can be matched the flow energy cannot. Thus thicker boundary layers will always be produced and separation likelihood will always be greater.

It has been established that boundary-layer transition has a significant influence on the flow-field of a wing operating in ground effect and it has been shown that modelling such events is not only important, but also possible with modern turbulence models.

ACKNOWLEDGEMENTS

The authors wish to thank Prof. Mark Drela of MIT for providing the MSES program for use in this study. The first author acknowledges the support of a Cranfield Defence and Security research bursary.

NOMENCLATURE

c	Wing chord /mm
C_D	Drag coefficient $\left(\frac{D}{q_\infty S}\right)$
C_F	Skin friction coefficient $\left(\frac{\tau}{q_\infty}\right)$
C_L	Lift coefficient $\left(\frac{L}{q_\infty S}\right)$
C_P	Pressure coefficient $\left(\frac{\Delta P}{q_\infty}\right)$
ΔC_P	Difference in pressure coefficient $(C_{P_{FREE-Transition}} - C_{P_{FORCED-Transition}})$

D	Drag force /N
h	Ground clearance /mm
L	Lift force (positive upwards) /N
K_L	Laminar kinetic energy /kg m ² s ⁻²
K_T	Turbulent kinetic energy /kg m ² s ⁻²
ΔK_T	Difference in turbulent kinetic energy ($K_{T_{FREE-Transition}} - K_{T_{FORCED-Transition}}$) /kg m ² s ⁻²
P	Local static pressure /Nm ⁻²
ΔP	Local static pressure relative to freestream /Nm ⁻²
P_0	Total pressure ($P + q_\infty$) /Nm ⁻²
ΔP_0	Difference in total pressure ($P_{0_{FREE-Transition}} - P_{0_{FORCED-Transition}}$) /Nm ⁻²
q_∞	Freestream dynamic pressure /Nm ⁻²
$RANS$	Reynolds-Averaged Navier-Stokes
Re	Chord-based Reynolds number ($\frac{U_\infty c}{\nu}$)
Re_θ	Momentum-thickness Reynolds number ($\frac{U_\infty \theta}{\nu}$)
S	Wing planform area /m ²
U_∞	Freestream velocity /ms ⁻¹
U_*	Shear velocity ($\sqrt{\frac{\tau}{\rho}}$) /ms ⁻¹
x, y, z	Cartesian coordinates (x – downstream, y – vertically up, z - horizontally)
y_N	Perpendicular distance from wall /m
Y^+	Dimensionless wall distance ($\frac{U_* y_N}{\nu}$)
δ^*	Boundary-layer displacement thickness /m
θ	Momentum thickness /m
ν	Kinematic viscosity /m ² s ⁻¹
ρ	Density /kg m ⁻³
τ	Local wall shear stress /Nm ⁻²
ω	Specific turbulence dissipation rate /s ⁻¹

REFERENCES

- [1] Mabey, D. G., 1991, "A Review of Scale Effects in Unsteady Aerodynamics," In Prog. Aerospace Sci, 28(4), pp. 273-321.
- [2] Knowles, K., Donogue, D. T., and Finnis, M. V., 1994, "A Study of Wings in Ground Effect," RAeS Vehicle Aerodynamics Conference, Loughborough.
- [3] Ranzenbach, R., and Barlow, J. B., 1994, "Two-Dimensional Airfoil in Ground Effect, An Experimental and Computational Study," SAE Technical Paper 942509.
- [4] Ranzenbach, R., and Barlow, J. B., 1995, "Cambered Airfoil in Ground Effect - Wind Tunnel and Road Conditions," AIAA Paper 95-1909, 13th Applied Aerodynamics Conference, San Diego, CA, USA.
- [5] Ranzenbach, R., and Barlow, J. B., 1996, "Cambered Airfoil in Ground Effect: An Experimental and Computational Study," SAE Technical Paper 942509, International Congress & Exposition, Detroit, MI.
- [6] Ranzenbach, R., and Barlow, J. B., 1997, "Multi-element Airfoil in Ground Effect - An Experimental and Computational Study," AIAA paper 97-2238, 15th Applied Aerodynamics Conference, Atlanta, GA, USA.
- [7] Zerihan, J. and Zhang, X., 2004, "Aerodynamics of a Single-Element Wing in Ground Effect," Journal of Aircraft, 37(6), pp. 1058-1064.
- [8] Correia, J., Roberts, L. S., Finnis, M. V. and Knowles, K., 2014, "Scale Effects on a Single-Element Inverted Wing in Ground Effect," The Aeronautical Journal, 118(7), pp. 797-809.
- [9] Mueller, T. J. and Batill, S. M., 1982, "Experimental Studies of Separation on a Two-Dimensional Airfoil at Low Reynolds Numbers," AIAA Journal, 20(8), pp. 457-463.

- [10] Huber, A. F., and Mueller, T. J., 1986, "The Effect of Grid Roughness on the Performance of the Wortmann FX 63-137 Airfoil at a Chord Reynolds number of 100,000," Proceedings of the Aerodynamics at Low Reynolds Number $10^4 < Re < 10^6$ International Conference, Royal Aeronautical Society, London.
- [11] Bloch, D. R., and Mueller, T. J., 1986, "Effects of Distributed Grit Roughness on Separation and Transition on an Airfoil at Low Reynolds Numbers," AIAA Paper 86-1788, 4th Applied Aerodynamics Conference, San Diego, CA, USA.
- [12] Lyon, C., Selig, M., and Broeren, A., 1997, "Boundary Layer Trips on Airfoils at Low Reynolds Numbers," AIAA Paper 97-0511, 35th Aerospace Sciences Meeting & Exhibit, Reno, NV, USA.
- [13] Horton, H. P., 1968, "Laminar Separation Bubbles in Two and Three Dimensional Incompressible Flow," PhD Thesis: University of London.
- [14] Knowles, K., and Finnis, M. V., 1998, "Development of a New Open-jet Wind Tunnel and Rolling Road Facility," 2nd MIRA International Conference on Vehicle Aerodynamics, Coventry, UK.
- [15] Moffat, R. J., 1988, "Describing the Uncertainties in Experimental Results," Experimental Thermal and Fluid Science, 1(1), pp. 3-17.
- [16] Braslow, A., and Knox, E., 1958, "Simplified Method for Determination of Critical Height of Distributed Roughness Particles for Boundary-Layer Transition at Mach Numbers from 0 to 5," NACA Report 4363, Langley Aeronautical Laboratory.
- [17] von Doenhoff, A. E., and Horton, E. A., 1958, "A Low-speed Investigation of the Effect of a Sandpaper Type of Roughness on Boundary Layer Transition," NACA Report 1349, Langley Aeronautical Laboratory.

- [18] Klebanoff, P. S., and Tidstrom, K. D., 1972, "Mechanism by Which a Two-dimensional Roughness Element Induces Boundary Layer Transition," *Physics of Fluids*, 15(7), pp. 1173-1188.
- [19] Drela, M., and Giles, M. B., 1987, "Viscous-Inviscid Analysis of Transonic and Low Reynolds Number Airfoils," *AIAA Journal*, 25(10), pp. 1347-1355.
- [20] Drela, M., 1993, "Design and Optimisation Method for Multielement Airfoils," *AIAA Paper 93-0960*, Aerospace Design Conference, Irvine, CA, USA.
- [21] van Ingen, J. L., 1956, "A Suggested Semi-empirical Method for the Calculation of Boundary Layer Transition Region," Report VTH-74, Delft University of Technology, Netherlands.
- [22] Smith, A. M. O., and Gamberoni, N., 1956, "Transition, Pressure Gradient and Stability Theory," Technical Report ES-26388, Douglas Aircraft Company.
- [23] Mack, L. M., 1977, "Transition Prediction and Linear Stability Theory," In *AGARD Laminar-Turbulent Transition 22*.
- [24] Correia, J., Roberts, L. S., Finnis, M. V., and Knowles, K., 2014, "Aerodynamic Characteristics of a Monoposto Racing Car Front Wing Operating in High Turbulence Conditions," *International Vehicle Aerodynamics Conference*, Paper C1385 015, Loughborough, UK. IMechE.
- [25] ANSYS Fluent, Release 15.0.07, 2014, 2600 ANSYS Drive, Canonsburg, PA 15317, USA. www.ansys.com
- [25] Zhang, X., Zerihan, J., Ruhrmann, A., and Deviese, M., 2002, "Tip Vortices Generated by a Wing in Ground Effect," *11th International Symposium on Applications of Laser Techniques to Fluid Mechanics*, Lisbon, Portugal.

Figure 1 - Schematic of a laminar separation bubble [13] 29

Figure 2 – Wind tunnel model: (a) wing profile and co-ordinate system; (b) assembly.	29
Figure 3 – Computational domain with boundary conditions indicated. Cell zones colored as laminar (upstream region) and turbulent (downstream region).	29
Figure 4 - Downforce and drag curves at varying non-dimensional ground clearances at $Re = 1.63 \times 10^5$, $Re = 2.03 \times 10^5$ and $Re = 2.44 \times 10^5$	30
Figure 5 - Flow visualisation of the suction surface at $Re = 1.63 \times 10^5$ (top) and $Re = 2.44 \times 10^5$ (bottom) for a) free transition and forced transition at b) $x/c = 0.1$, c) $x/c = 0.3$, and d) $x/c = 0.5$ (flow moving top to bottom, $h/c = 0.3125$)	31
Figure 6 - Flow visualisation of the suction surface at $Re = 1.63 \times 10^5$ for a) free transition and forced transition at b) $x/c = 0.1$, c) $x/c = 0.3$, and d) $x/c = 0.5$ (flow moving top to bottom, $h/c = 0.125$)	31
Figure 7 - MSES results for force coefficients at free transition and varying trip locations (forced transition) at $h/c = 0.3125$ ($Re = 2.44 \times 10^5$).	32
Figure 8 - Streamlines around the airfoil section with forced transition at a) 0.1c, b) 0.3c, and c) 0.5c and d) free transition, computed in MSES ($h/c = 0.3125$, $Re = 2.44 \times 10^5$).	32
Figure 9 - MSES results for suction surface: a) pressure, b) skin friction, c) boundary-layer displacement thickness, and d) momentum-thickness Reynolds number for free transition and varying trip location ($h/c = 0.3125$, $Re = 2.44 \times 10^5$).	33
Figure 10 - Comparison of experimental (left) and CFD (right) surface streamlines for free transition (top) and transition forced at $x/c = 0.1$ (bottom) ($h/c = 0.3125$, $Re = 2.44 \times 10^5$). ...	34
Figure 11 – RANS results for a) pressure distribution about wing, and b) x-component of shear stress on suction surface of wing at $z/s = 0$ for free- and forced-transition cases ($h/c = 0.3125$, $Re = 2.44 \times 10^5$).	34
Figure 12 - Contours of a-b) static pressure coefficient, c-d) total pressure loss, and e-f) turbulent kinetic energy for free-transition (left) and the difference between the free- and forced-transition cases (right) ($h/c = 0.3125$, $Re = 2.44 \times 10^5$).	35

Table 1 - Downforce and drag coefficients, and boundary-layer separation and reattachment locations for free- and forced-transition wing from experiments and CFD.....	20
--	----

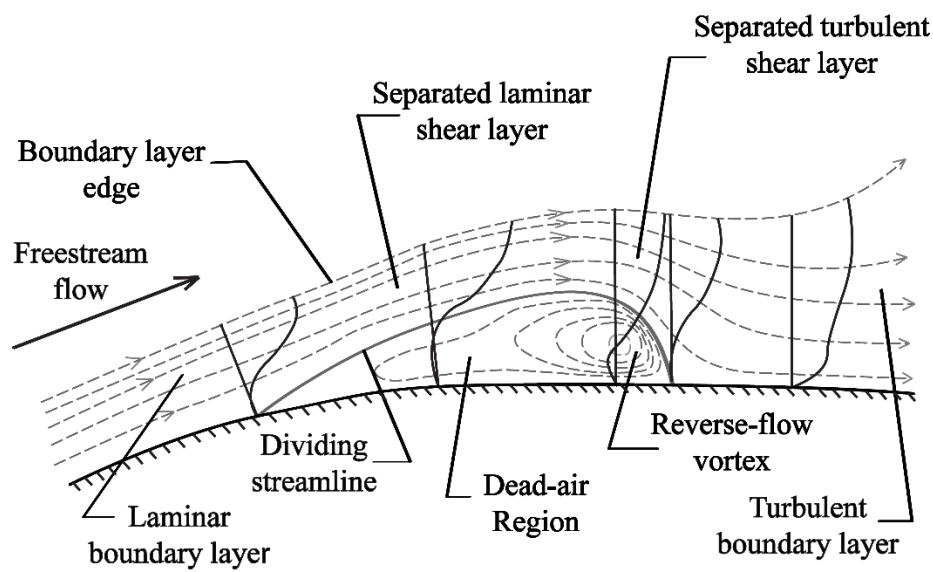


Figure 1 - Schematic of a laminar separation bubble [13]

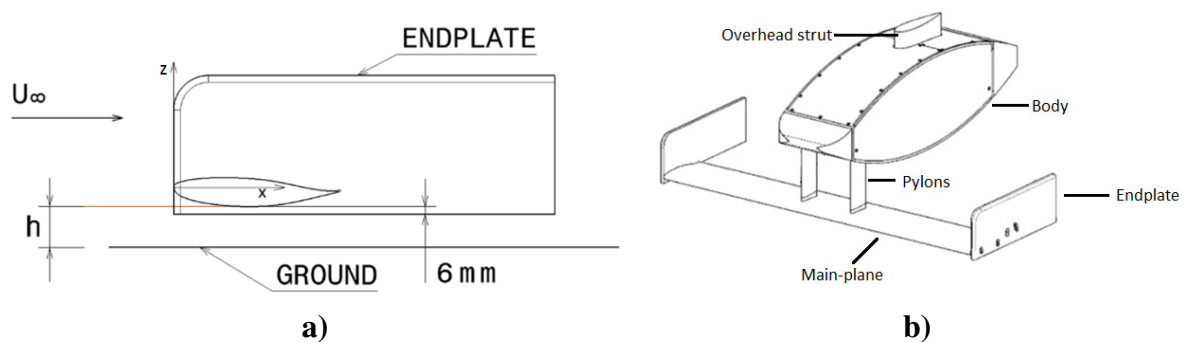


Figure 2 – Wind tunnel model: (a) wing profile and co-ordinate system; (b) assembly.

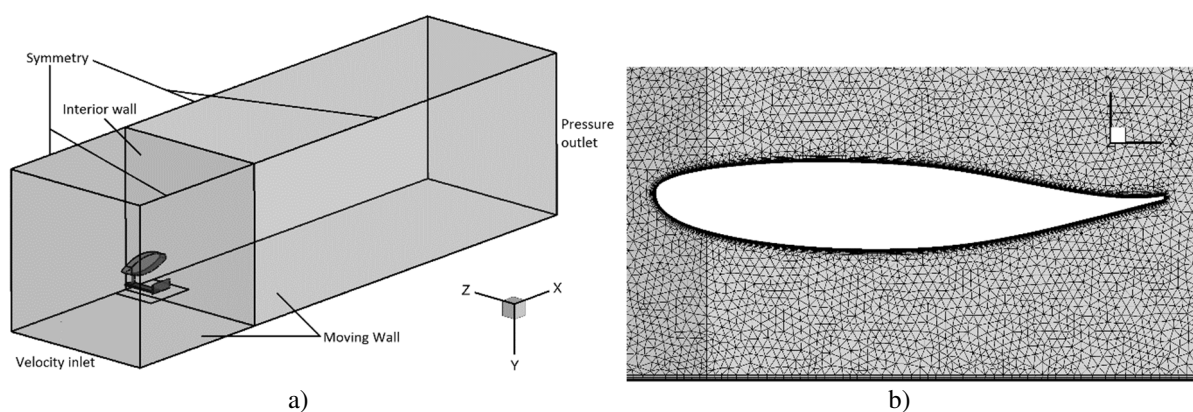


Figure 3 – Computational domain with boundary conditions indicated. Cell zones colored as laminar (upstream region) and turbulent (downstream region).

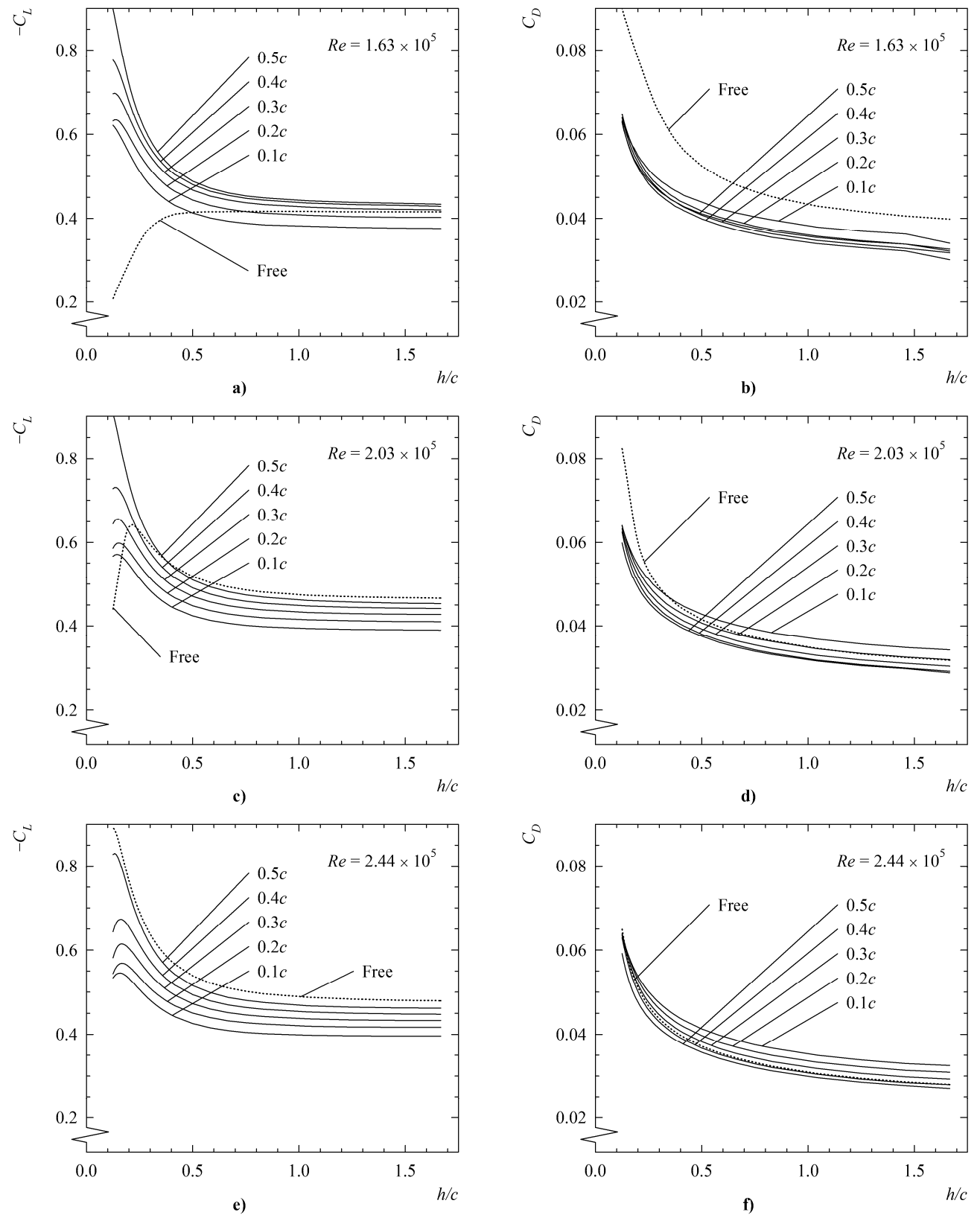


Figure 4 - Downforce and drag curves at varying non-dimensional ground clearances at $Re = 1.63 \times 10^5$, $Re = 2.03 \times 10^5$ and $Re = 2.44 \times 10^5$

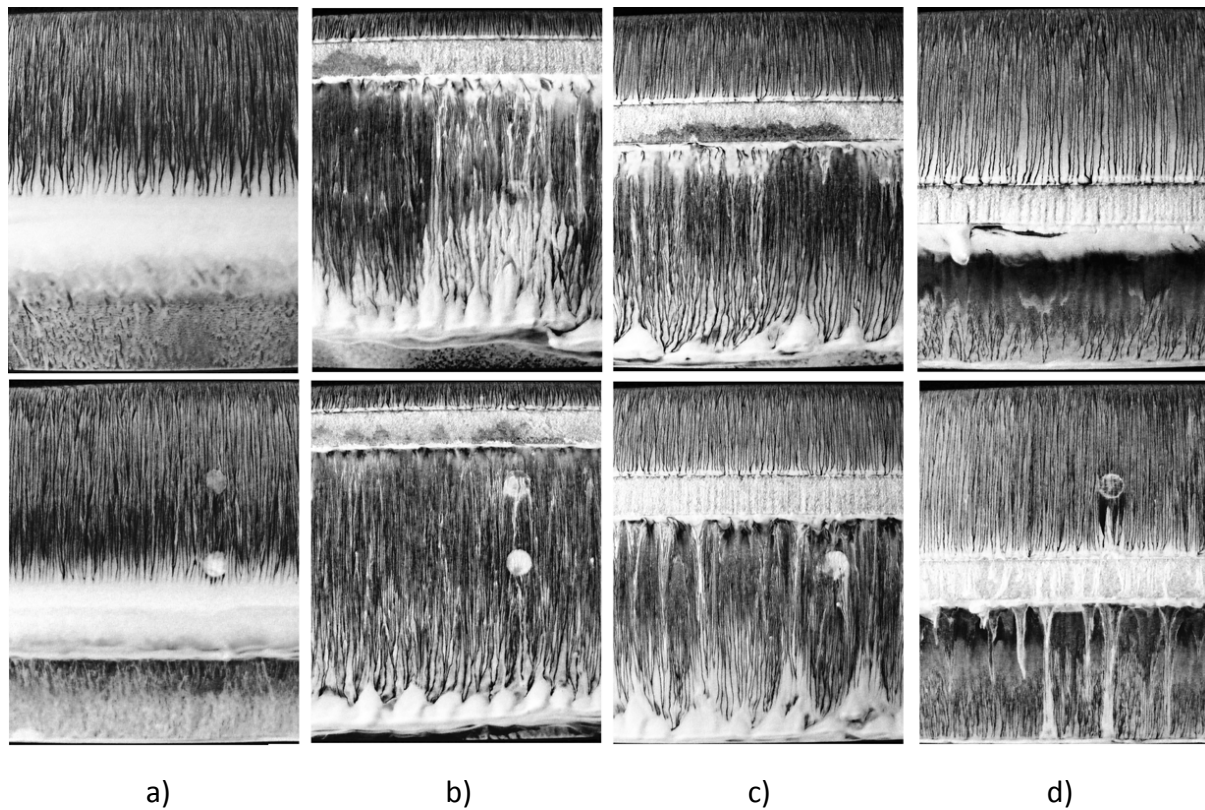


Figure 5 - Flow visualisation of the suction surface at $Re = 1.63 \times 10^5$ (top) and $Re = 2.44 \times 10^5$ (bottom) for a) free transition and forced transition at b) $x/c = 0.1$, c) $x/c = 0.3$, and d) $x/c = 0.5$ (flow moving top to bottom, $h/c = 0.3125$)

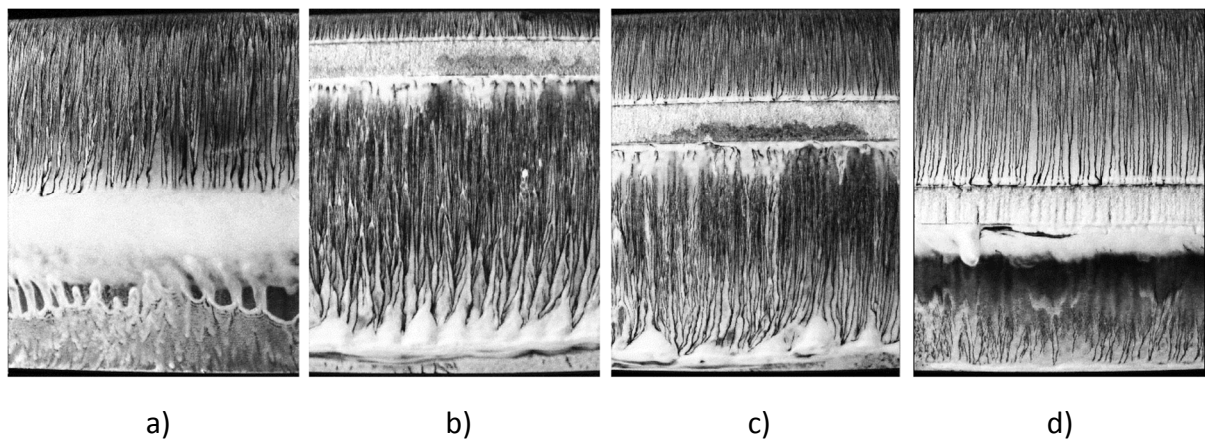


Figure 6 - Flow visualisation of the suction surface at $Re = 1.63 \times 10^5$ for a) free transition and forced transition at b) $x/c = 0.1$, c) $x/c = 0.3$, and d) $x/c = 0.5$ (flow moving top to bottom, $h/c = 0.125$)

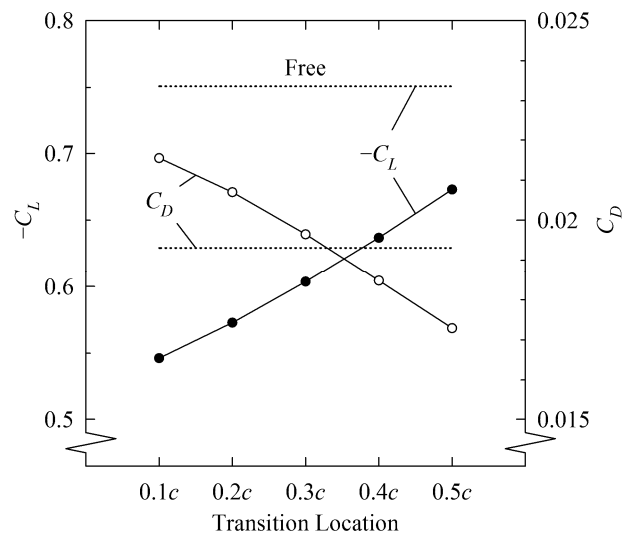


Figure 7 - MSES results for force coefficients at free transition and varying trip locations (forced transition) at $h/c = 0.3125$ ($Re = 2.44 \times 10^5$).

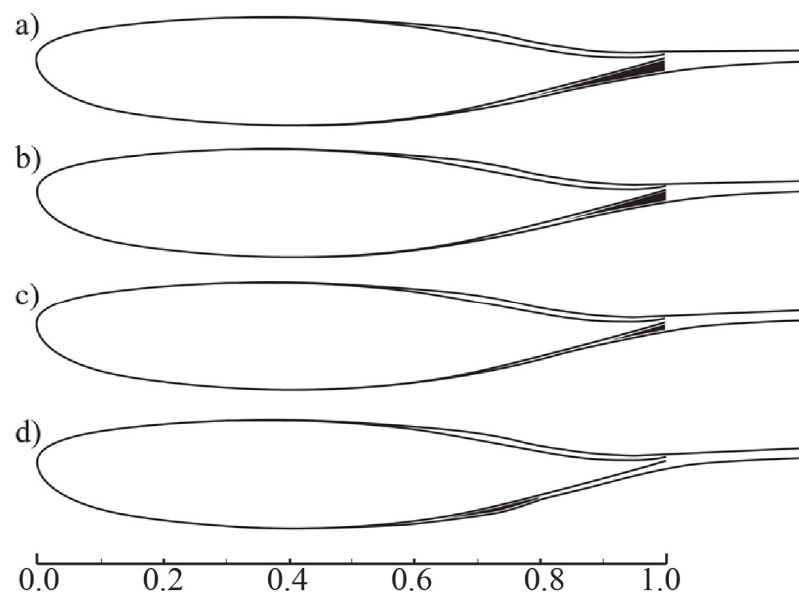


Figure 8 - Streamlines around the airfoil section with forced transition at a) 0.1c, b) 0.3c, and c) 0.5c and d) free transition, computed in MSES ($h/c = 0.3125$, $Re = 2.44 \times 10^5$).

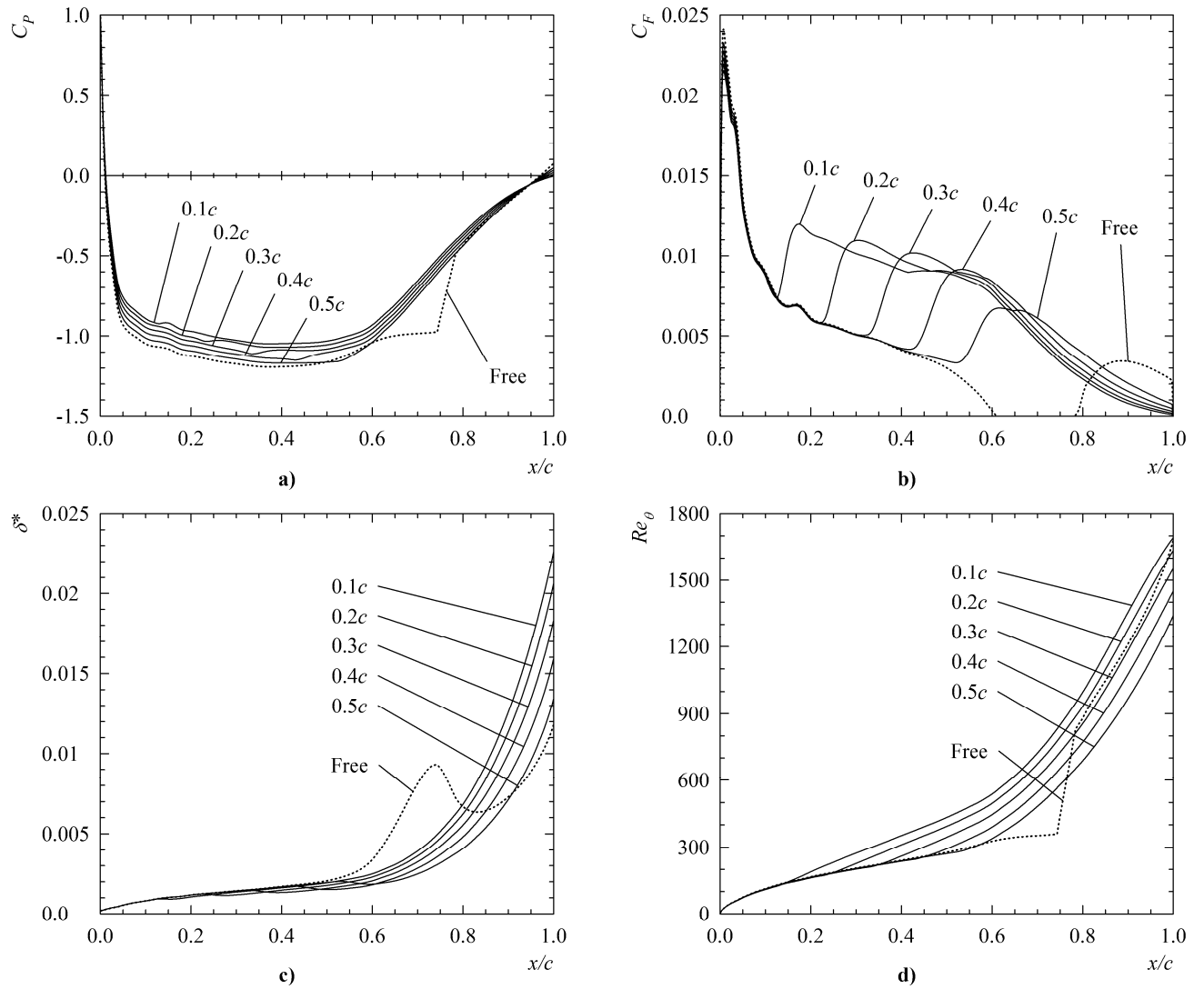


Figure 9 - MSES results for suction surface: a) pressure, b) skin friction, c) boundary-layer displacement thickness, and d) momentum-thickness Reynolds number for free transition and varying trip location ($h/c = 0.3125$, $Re = 2.44 \times 10^5$).

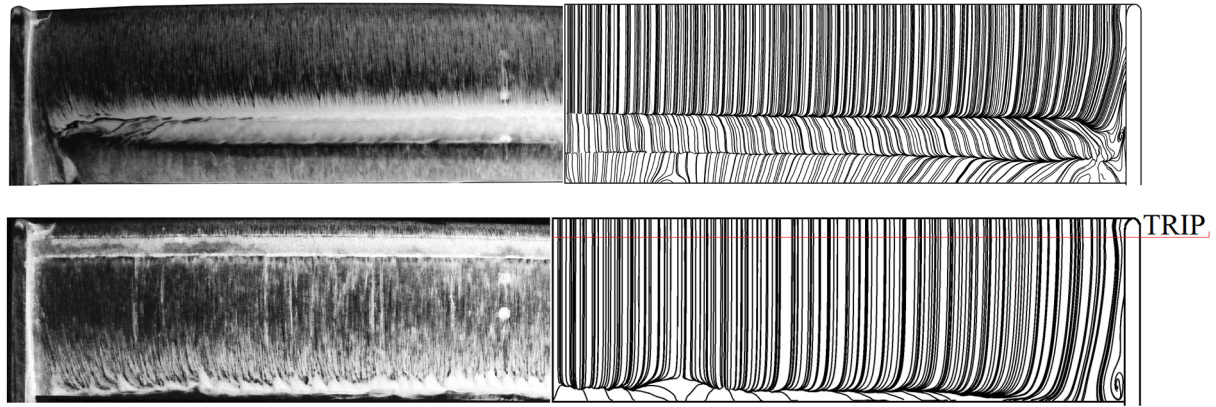


Figure 10 - Comparison of experimental (left) and CFD (right) surface streamlines for free transition (top) and transition forced at $x/c = 0.1$ (bottom) ($h/c = 0.3125$, $Re = 2.44 \times 10^5$).

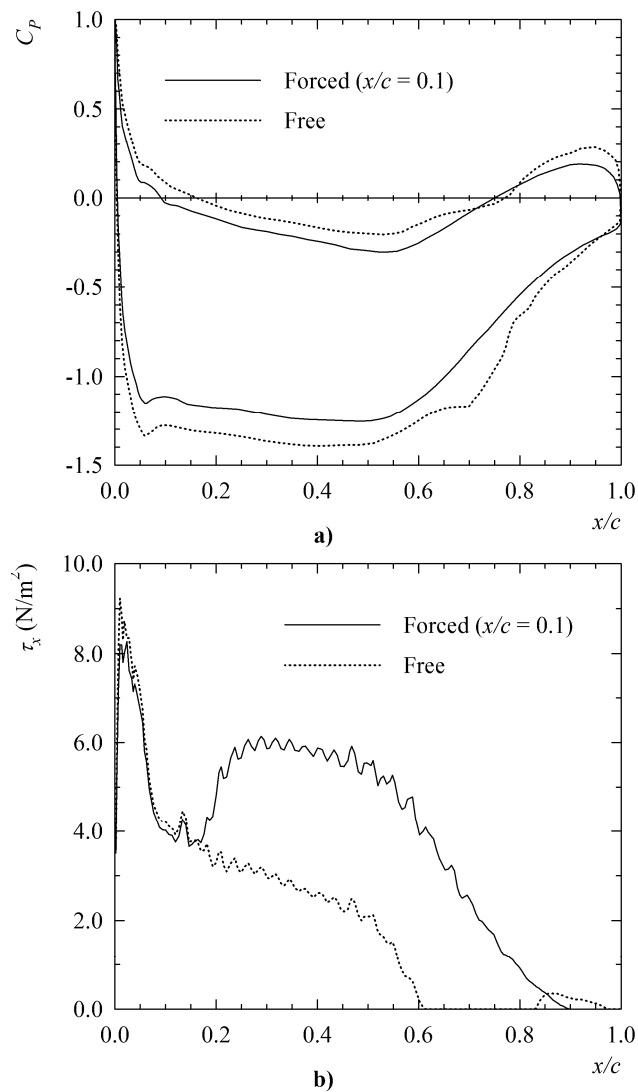


Figure 11 – RANS results for a) pressure distribution about wing, and b) x-component of shear stress on suction surface of wing at $z/s = 0$ for free- and forced-transition cases ($h/c = 0.3125$, $Re = 2.44 \times 10^5$).

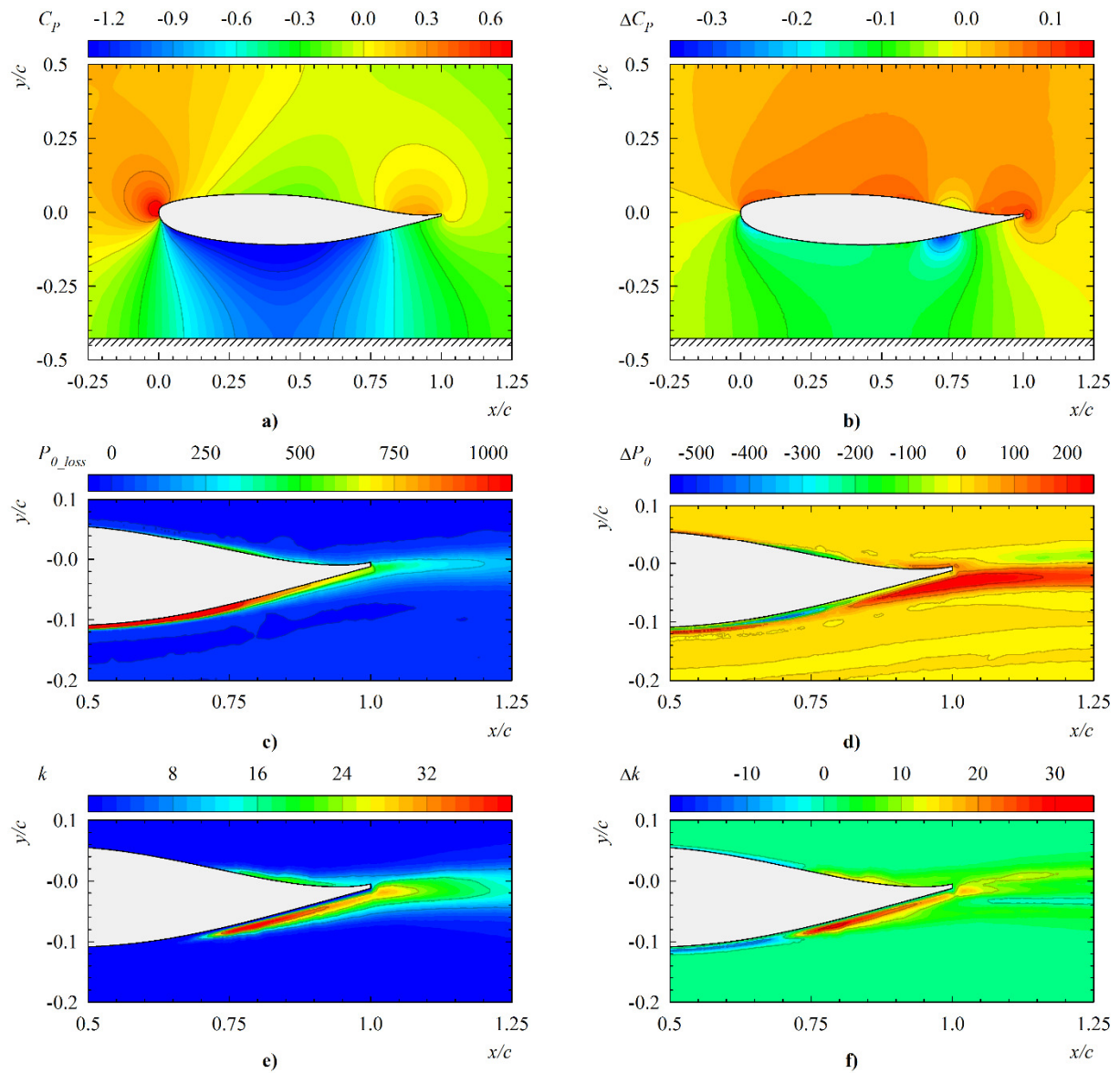


Figure 12 - Contours of a-b) static pressure coefficient, c-d) total pressure loss, and e-f) turbulent kinetic energy for free-transition (left) and the difference between the free- and forced-transition cases (right) ($h/c = 0.3125$, $Re = 2.44 \times 10^5$).

Forcing boundary-layer transition on a single-element wing in ground effect

Roberts, Luke S.

2017-06-14

Attribution 4.0 International

Roberts LS, Finnis MV, Knowles K. (2017) Forcing boundary-layer transition on a single-element wing in ground effect. *Journal of Fluids Engineering*, Volume 139, Issus 10, October 2017, Article number 101205

<http://dx.doi.org/10.1115/1.4037036>

Downloaded from CERES Research Repository, Cranfield University